12-1-2004

Self-consistent Diffusive Lifetimes of Weibel Magnetic Fields in Gamma-Ray Bursts

C. H. Jaroschek
Max Planck Institute for Extraterrestrial Physics

H. Lesch
Max Planck Institute for Extraterrestrial Physics

R. A. Treumann
Dartmouth College

The Astrophysical Journal, 616:1065–1071, 2004 December 1

SELF-CONSISTENT DIFFUSIVE LIFETIMES OF WEIBEL MAGNETIC FIELDS IN GAMMA-RAY BURSTS

C. H. Jaroschek,[1,2] H. Lesch,[1,2] and R. A. Treumann[1,3]

Received 2004 June 17; accepted 2004 August 6

ABSTRACT

Weibel filamentation in relativistic plasma shell collisions has been demonstrated as an efficient and fast mechanism for the generation of near-equipartition magnetic fields in self-consistent particle-in-cell (PIC) simulations. In generic γ-ray burst (GRB) models with kinetically dominated plasma outflow, sufficient strength and lifetime of magnetic fields are essential to validate synchrotron emission as the source of radiative outbursts. In this article we report on self-consistent PIC simulations of pair-plasma shell collisions in the highly relativistic regime with particle ensembles up to 5×10^8. Energy dependence of magnetic field generation in the Weibel process is discussed, and for the first time the diffusion-limited lifetime of magnetic fields is investigated self-consistently. In three different analyses the diffusion coefficient is determined self-consistently from the microphysical particle data. Cross-field diffusion is identified as "Bohm"-type by direct confirmation of the characteristic T/B-behavior. With the stability-limiting process pinned down, the lifetime of Weibel magnetic fields in plasma shell collisions subsumes to $\tau\omega_{p0} \sim 10^9$ (with ω_{p0} the plasma inertial timescale as characteristic of any system). In the context of typical synchrotron cooling times, we conclude that the Weibel fields are sufficiently long-lived for GRB prompt emission as well as afterglows, especially in view of the likely "baryonic" pollution of pair-plasma shells.

Subject headings: acceleration of particles — gamma rays: bursts — instabilities — magnetic fields — plasmas

1. INTRODUCTION

The generation and stability of magnetic fields in γ-ray bursts (GRBs) remains a central problem of all theoretical concepts to explain the enormous radiation deposition in such phenomena. In principle, two plasma physical mechanisms qualify to generate magnetic fields of sufficient strength for synchrotron emission models to work: magnetic field amplification via shock compression (Kazimura et al. 1998) and Weibel filamentation (Medvedev & Loeb 1999) in plasma shell collisions. Both processes rely on the interaction of counterstreaming plasmas.

Conceptual GRB emission models (for an extensive review of GRBs, see Piran 1999 and Mészáros 2002) propose a central source ejecting plasma shells at variable bulk speeds and intermittences. Differences in bulk speed cause individual plasma shells to collide at some distance from the central object. In close similarity to the so-called corotating interaction regions (CIR) in the solar wind, high Mach number shock fronts are triggered at the face of the interaction regions. However, although shock compression provides magnetic field strengths close to equipartition, Gruzinov (2001) presented arguments that the shock-amplified fields decay rapidly in the zone downstream of the shock front. Direct numerical simulations indicate short magnetic field lifetimes on the order of a few tens of plasma dynamic scales ω_p^{-1}, whereas generic synchrotron emission scenarios take place on longer timescales, ranging from 10^5 to 10^{10} ω_p^{-1}.

The alternative approach of Weibel-induced magnetic fields refers to the counterstreaming motion of deeply interpenetrating plasma shells: shock compression is spatially confined within the narrow zone of the shock front propagating as the wake of plasma interaction into the colliding shells. Counterstreaming develops downstream as a consequence of the progressive interchange of the shells' bulk momentum and downstream advection of electromagnetic fields, and hence characterizes merely the late evolution of shock scenarios (Frederiksen et al. 2004). We note that for typical source environments the plasma is strongly rarefied in density. Consequently, the term "collision" refers to particle scattering effective in the collective potentials of plasma instabilities (Sagdeev 1979) rather than to Coulomb interaction between nearest neighbors.

The Weibel mechanism (Weibel 1959) relies on the free energy stored in a particle distribution that is anisotropic in velocity space. Counterstreaming plasma shells represent an extreme case of velocity anisotropy. Each moving charge represents a current. Parallel currents are mutually attractive. Small initial perturbations likewise cause currents to merge and form small incipient current filaments. Therefore, the Weibel instability is also called filamentation instability. We present a scenario of counterstreaming pair-plasma shells with equal density and equal absolute bulk momentum. As a consequence, the configuration is initially charge and current neutral in the center-of-mass frame (i.e., simulation or lab frame). Current filaments consist of equal charges moving parallel in one shell and respectively opposite charges moving antiparallel as constituents of the counterstreaming shell. Filaments remain quasi-neutral and sustain a toroidal magnetic field. The toroidal field self-pinches its generating current, thereby amplifying the current and closing the instability feedback loop. Separation of self-pinches is determined by the fastest growing Weibel mode. The toroidal magnetic fields of individual filaments superpose to complex field structures predominantly oriented transverse to the respective currents. Particles perform

[1] Center for Interdisciplinary Plasma Science, Max-Planck-Institut für extraterrestrische Physik, Giessenbachstrasse Postfach 1603, Garching 85748, Germany; cjarosch@mpe.mpg.de, tre@mpe.mpg.de.

[2] Observatory of the Ludwig-Maximilian-University, Scheinerstrasse 1, Munich 81679, Germany; lesch@usm.uni-muenchen.de.

[3] Department of Physics and Astronomy, Dartmouth College, 6127 Wilder Laboratory, Hanover, NH 03755.

a meandering motion in the toroidal field confinement. The instability saturates as soon as the bounce frequency associated with the meandering becomes comparable to the instability growth (Silva et al. 2003). Self-consistent particle-in-cell (PIC) simulations of the Weibel instability in electron–positron (e^-, e^+) shell collisions (Silva et al. 2003) proved its capacity to generate near-equipartition magnetic fields. Since sufficient strength of the newly generated fields is granted, the critical question to be answered concerns the stability of the Weibel magnetic fields.

In this article we investigate the finite lifetime of Weibel-generated magnetic fields in relativistic plasma shell collisions. The highly nonlinear late-time evolution of plasma instabilities is the condition prevalent on astrophysical timescales, and direct numerical simulation is one possible approach to explore this regime. The PIC method allows us to simulate the Weibel instability on the plasma kinetic level and to trace the individual trajectories of particles self-consistently involved in the generation of the fields. These are essential differences with respect to test-particle approaches. Since the process is manifestly collisionless, the destruction of the magnetic fields can only take place by scattering of the current-carrying particles in the field inhomogeneities and by intrinsic instabilities. This should lead to diffusive losses of particles from the current filaments and thus to destruction of the current-field configuration. In order to determine the importance and timescales of this kind of diffusion, we harness the data of individual particle orbits to analyze the mechanism of magnetic cross-field diffusion. We further note that contributions to cross-field decay can also arise from flute instabilities of the Kelvin-Helmholtz–, sausage-, kink-, or pinch-type. Such instabilities modify the current-field configuration on length scales that require global scenarios and thus are beyond the feasibility of self-consistent kinetic simulations. We focus here on the microphysics to investigate the fundamental mechanism of cross-field transport and the timescales involved.

It is essential to simulate three-dimensional configurations because of two constraints. First, up to the moderately relativistic collision energies $\gamma_0 \sim 10$ assumed in internal shell collision scenarios, the current filaments exhibit an intrinsic three-dimensional structure (Silva et al. 2003). Three-dimensional elements arise from the energy-dependent coupling between the Weibel mode (effective perpendicular to the collision-aligned direction) and the parallel two-stream instability mode. For external shell-collision energies with Lorentz factors inferred from GRB light curves around $\gamma_0 \sim 100$ (Panaitescu & Kumar 2002), the coupling strength between the two instability modes softens. The Weibel contributions prevail instead, and the current filament/magnetic field structure becomes quasi–two-dimensional (Jaroschek et al. 2004a). However, the particle trajectories maintain a distinctively complex three-dimensional pattern. Second, even in entirely two-dimensional magnetic field configurations it is a fundamental insight that perpendicular transport requires a three-dimensional configuration (Jokipii et al. 1993).

Details on the PIC simulation setup are described in § 2. In § 3 we show that the lifetime of the final steady state magnetic fields generated in the Weibel process is limited by magnetic cross-field diffusion. Meticulous analysis of individual self-consistent particle trajectories allows (1) the concise determination of the diffusion coefficient and (2) the identification of the diffusion mechanism as "Bohm"-type, and hence qualifying it as the conservative upper limit of particle transport. The diffusion coefficient obtained in the self-consistent PIC simulation renders feasible magnetic field lifetimes of $\sim 10^9 \omega_p^{-1}$ in ultrarelativistic plasma shell collisions. This credences the validity of Weibel-generated magnetic fields in the context of conceptual GRB synchrotron emission models.

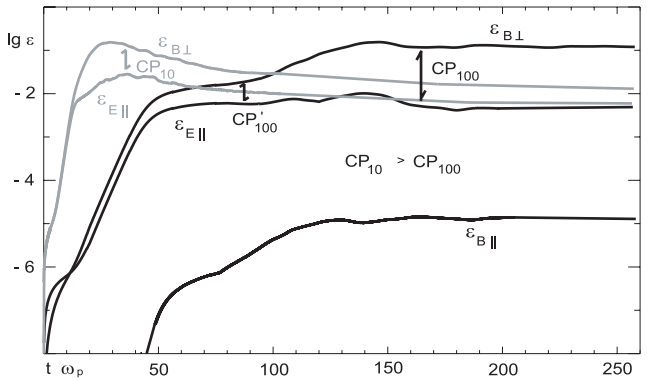

FIG. 1.—*Gray lines*: Time evolution of equipartition ratios for γ_0^{10} with linear growth until decoupling at $t_1\omega_{p0} = 13$, saturation at $t_2\omega_{p0} = 27$, and final steady state for $t_2\omega_{p0} > 130$. *Black lines*: Time evolution of equipartition ratios for γ_0^{100} with linear growth until decoupling at $t_1\omega_{p0} = 42$, saturation at $t_2\omega_{p0} = 140$, and final steady state for $t_2\omega_{p0} > 190$. The coupling strength in the two-dimensional TSI-WBI mode weakens from γ_0^{10} to γ_0^{100}, i.e., $CP_{10} > CP_{100}$. Longitudinal $B_\parallel$ contributions are always negligible. As final equipartition ratios, we find $\epsilon_B^{10} \sim 2.5\%$ and $\sim 12\%$.

2. SIMULATION DESCRIPTION

The PIC simulations serving as foundation for the present study are similar to the ones described in Jaroschek et al. (2004a). For completeness we summarize the simulation setup: the simulations are performed with a massively parallelized, relativistic, fully electromagnetic PIC code on a high-resolution mesh with $256 \times 256 \times 128$ grid points representing a three-dimensional system of extension $L_x \times L_y \times L_z = 25.6 \times 25.6 \times 12.8(c/\omega_{p0})^3$. The total number of particles subsumes to 5×10^8, homogeneously distributed in configuration space and divided in phase space into two equal subensembles initially moving in $\pm z$ with $v_{z0,1} = -v_{z0,2}$. Each subensemble represents a quasi-neutral (e^+, e^-) shell of density $n_0^+ = n_0^- = n_0$. Times are normalized to the inverse plasma frequency $\omega_{p0}^{-1} = (4\pi e^2 n_0/m)^{-1/2}$, lengths to the skin depth (c/ω_{p0}), and, as a consequence thereof, velocities to the speed of light c. Here n_0 is the initial density of one specie within a particular shell, and e and m are electron charge and mass, respectively. Initial bulk motions correspond to $\gamma_0^{10} v_{z,0} = 10.00$ and $\gamma_0^{100} v_{z,0} = 100.00$. The transverse thermal spread in the shells' comoving frame is $v_{\mathrm{th},0} = 10^{-4}$, corresponding to $v_{\mathrm{th},0}^{10} = 10^{-5}$ and $v_{\mathrm{th},0}^{100} = 10^{-6}$ in the lab (= grid mesh) frame. Simulations endured for $\Delta t\omega_{p0} = 260$, requiring 5500 time steps for γ_0^{10} and 45,000 time steps for γ_0^{100} to assure energy stabilities of 0.1% and 1%, respectively.

The efficiency of magnetic field generation in the Weibel process is quantified in the equipartition ratio $\epsilon_B = V^{-1} \int dV (B^2/8\pi)/\mu_{\mathrm{kin}}$, i.e., the energy density on average converted into magnetic field B from an initial particle kinetic reservoir $\mu_{\mathrm{kin}} = 4(\gamma_0 - 1) n_0 mc^2$. Figure 1 shows the time evolution of $\epsilon_B^{10,100}$ for moderate γ_0^{10} and ultrarelativistic γ_0^{100} collision energy. Here $\epsilon_B^{10}(t)$ is precisely consistent with results of Silva et al. (2003) and corresponds to the regime of internal (prompt emission) GRB shell collisions. First, $\epsilon_B^{100}(t)$ probes the regime of external (afterglow) collisions. In general

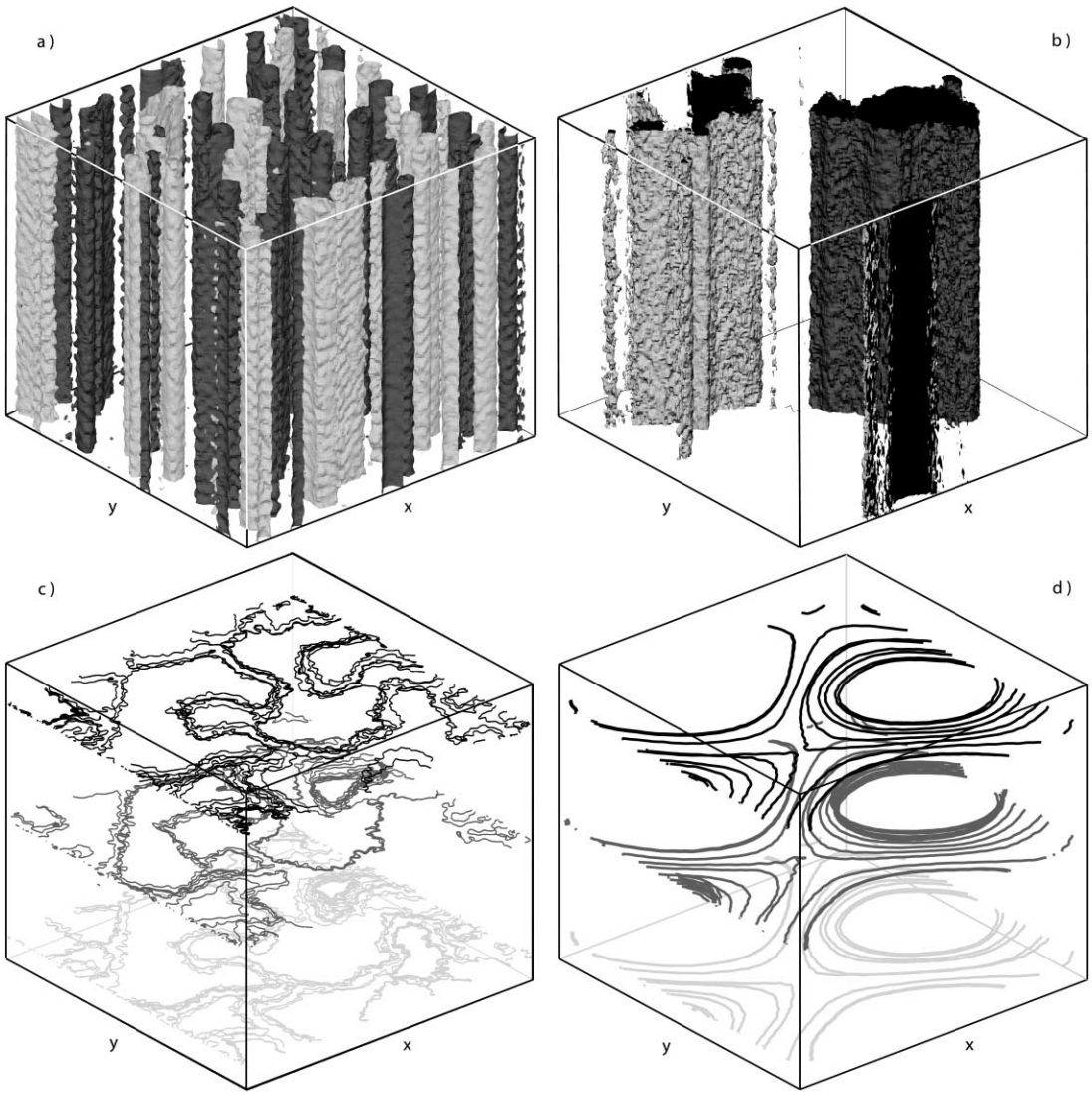

FIG. 2.—(*a*) Isocontours of the current density for γ_0^{100} in the maximum self-pinched state at $t\omega_{p0} = 140$. (*b*) Coalescence of self-pinches ceases as soon as only oppositely aligned currents ($j_z > 0$, *dark region*; $j_z < 0$, *bright region*) neighbor each other and the final steady state configuration is reached for $t\omega_{p0}^{-1} > 190$. The corresponding magnetic field configurations are visualized in (*c*) and (*d*), respectively. Spatial agglomeration of the field lines reflects the magnetic energy distribution. Filaments are confined within the self-generated quasi–two-dimensional toroidal magnetic fields (for clarity, only shown in three staggered planes). Around each filament magnetic fields are close to equipartition. The typical correlation scale of the current-field configuration evolves exponentially in time from large to small wavenumbers k (cf. Fig. 4).

the plasma instability is a coupled mode propagating at a skewed angle with a two-stream (TSI) and Weibel (WBI) constituent, each effective exactly parallel and perpendicular to the bulk motion, respectively. As reported in detail in Jaroschek et al. (2004a), WBI contributions responsible for the conversion of particle-kinetic into magnetic-field energy progressively dominate the TSI contributions for higher collision energies, the latter associated with parallel electric fields and plasma heating. As a direct consequence, the final steady state magnetic field strength is higher in the ultrarelativistic limit (cf. Fig. 1). In plasma-physical terms, the propagation angle of the coupled TSI-WBI mode becomes quasi-perpendicular, while the current filament/magnetic field structure becomes quasi–two-dimensional (Fig. 2). We note in passing that the coupled TSI-WBI mode in any energy regime remains a real three-dimensional problem at late times, when filaments of like currents tend to merge and require the third dimension to circumnavigate their respective countercurrents; the latter are essential to ensure the system's time-invariant overall current neutrality (Lee & Lampe 1973).

3. DIFFUSION LIMITED LIFETIME OF MAGNETIC FIELDS

3.1. *Diffusion Coefficients Obtained in the PIC Simulation*

In the final steady state configuration only oppositely aligned current filaments neighbor each other, being confined within the voids of their self-generated toroidal magnetic fields (Fig. 2) and forming something like a quasi-stable lattice. Consequently, the magnetic field gradient and particle density exhibit minima in the magnetic walls separating the current filaments. This differs fundamentally from the situation of Harris-type cross-field diffusion scenarios (Jaroschek et al. 2004b). In the following discussion we concentrate on the case $\gamma_0 = 100$, because magnetic field topology then is essentially quasi–two-dimensional, and discuss three-dimensional modifications for less energetic

collisions in the end. Stability and lifetime limits of this configuration are imposed by cross-field diffusion between the Weibel current filaments. Perpendicular transport requires some perturbation along the particle's gyro orbit to break its "force-free" appendance to a specific field line. Since Coulomb collisions are absent, "anomalous" transport is retained by particles scattering off collective electromagnetic fluctuations. Electrostatic "convective cells" in thermalized plasma were identified as the origin of collisionless perpendicular diffusion within the framework of a guiding center $\boldsymbol{E}\times\boldsymbol{B}/B^2$ drift (zero frequency) limit by Taylor & McNamara (1971) and were then generalized by Dawson et al. (1971) to cover a broad spectral range of fluctuations. In the Weibel scenario, the dominant contributions to cross-field transport are expected to arise from density and/or magnetic field gradients. Self-consistent PIC simulations allow for the determination of a net diffusion coefficient $D_{\rm PIC}$ as gross yield of individual transport processes directly from the analysis of the particle data.

On the microphysical level, the diffusion coefficient is defined for each individual particle $D^*_{\rm PIC} = (\Delta x)^2/\Delta t$ as temporal path variance $(\Delta x)^2$ across the magnetic field. Figure 3*a* shows $(\Delta x)^2(t)$ for a selected individual particle. Significant path variations set on around $t\omega_{p0} \sim 130$ in coincidence with nonlinear magnetic field saturation (cf. Fig. 1). Here $(\Delta x)^2$ clearly represents the superposition of an oscillatory motion and a distinct cross-field drift. The oscillation describes the meandering of the particle within the magnetic voids in which each current filament is embedded. The toroidal magnetic field confines the particle, i.e., escaping current carriers are diverted reversely into the filament. The oscillation timescale is short compared to the cross-field drift but is straightforwardly removed in a linear regression line fit. The resulting slope of the fit corresponds to the cross-field diffusion $D^*_{\rm PIC} = 3.2\times10^{-5}(c^2/\omega_{p0})$ of the individual particle.

We determined $D^*_{\rm PIC}$ for a sample of 32,768 individual trajectories. The sample consists of two distinct classes. 20,472 particles constitute a first class, characterized by $D^*_{\rm PIC} < 0$, which corresponds to a particle ensemble being cooled and progressively confined within the magnetic voids. The second class contains all particles with $D^*_{\rm PIC} > 0$ exhibiting cross-field diffusion with average diffusion coefficient $D_{\rm PIC} = 9.6\times10^{-6}(c^2/\omega_{p0})$. The critical question in this analysis is whether the two classes are distinctly separated, i.e., whether the average diffusion coefficient is sharply defined. Figure 3*b* shows the normalized distribution of the class 2 particles around $D_{\rm PIC}$. Intriguingly, the rate of cross-field diffusion is reflected in a concise and unambiguous fashion in the self-consistent particle transport data.

In Figures 2*b* and 2*d* a steady state configuration is reached in which only oppositely aligned currents are neighbored. Cross-field diffusion describes the tendency of mutual annihilation of opposite currents, i.e., ohmic dissipation of the free energy stored in the currents by an "anomalous" resistivity $\bar{\eta}$. In a second line of argumentation, $\bar{\eta}$ serves as a cross-check for perpendicular transport: The dissipative ohmic power loss as average over the simulated volume subsumes to

$$\Pi_{\rm ohm} = -V^{-1}\int dV(\bar{\eta}\cdot\boldsymbol{j})_\perp\cdot\boldsymbol{j} = -V^{-1}\int dV\tilde{\boldsymbol{E}}_\perp\cdot\tilde{\boldsymbol{j}}.$$

Therein the local current density $\tilde{\boldsymbol{j}} = \sum_{\rm ppg} q_i\boldsymbol{v}_i$ is an ensemble quantity defined for each individual grid cell. The grid cell level is the most refined entity in configuration space.

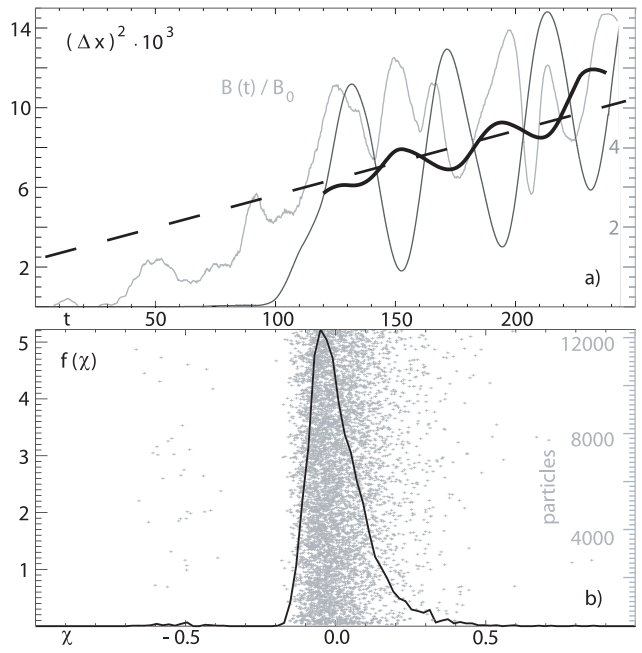

FIG. 3.—(*a*) Path variance $(\Delta x)^2(t)$ as function of time for an individual particle. For significant Weibel magnetic fields at the particle position (*gray line*), the trajectory is constituted by the superposition of the meandering motion within the magnetic confinement and a distinct cross-field drift. In order to subtract meandering, particle motion is smoothed (*thick black line*) and the slope of the respective regression line fit indicates a microphysical diffusion coefficient $D^*_{\rm PIC} = 3.2\times10^{-5}(c^2/\omega_{p0})$. (*b*) 37.5% of a subensemble of 32,768 trace particles shows cross-field diffusion with $\chi = \lg(D^*_{\rm PIC}/D_{\rm PIC})(\lg D_{\rm PIC})^{-1} = 0$ corresponding to a statistical average $D_{\rm PIC} = 9.6\times10^{-6}(c^2/\omega_{p0})$. Diffusing particles form a distinct class as seen from the sharp normalized distribution $f(\chi)$ around $D_{\rm PIC}$.

$\tilde{\boldsymbol{E}} = \sum\boldsymbol{E}_i/{\rm ppg}$ is the corresponding ensemble-averaged local electric field as superposition of values $\boldsymbol{E}_i$ interpolated to the respective positions of ppg (particles per individual grid cell). PIC simulations are systematically "noisy" with respect to electric field fluctuations. Such fluctuations are artificially introduced by the quasi-particle/field-grid representation (Birdsall & Langdon 1995). The number of quasi particles per grid cell (qpc) is the critical quantity with respect to the fluctuation level. We tested qpc-variations in the simulation setup to ensure that the model-inherent resistivity $\bar{\eta}_{\rm qpc} \ll \eta$ is not blending the results. The initial kinetic energy of the configuration is determined by the shells' bulk motion $\mu_{\rm kin} = 4(\gamma_0 - 1)n_0mc^2$ since the initial thermal spread is negligible. Anomalous dissipative losses define a "thermalization" decay timescale of the magnetic fields $\tau_\eta = -\mu_{\rm kin}/\Pi_{\rm ohm}$. Since the decay time $\tau_\eta \gg t_{\rm tot} \gg \delta t$ is large compared to the total simulated time $t_{\rm tot}$ and the time step δt, we can study the time evolution of $\tau_\eta(t)$ during the simulation. Most interesting is the direct correspondence to the time evolution of magnetic field structures, as shown in Figure 4. When Weibel filamentation sets in, the magnetic field is topologically characterized by large wavenumbers k (thus, small scales) and comparatively weak strengths. With consecutive coalescence of current filaments, structures migrate to smaller k, separative field strengths grow, and cross-field diffusion and anomalous resistivity weaken. The final (on simulation times) steady state configuration stabilizes at typical decay times around $\tau_\eta(t_{\rm fin})\omega_{p0} \sim 10^9$.

Intriguingly, this value is consistent with the cross-field diffusion $D_{\rm PIC}$ obtained from the microphysical analysis of self-consistent particle motion. Since filaments are roughly

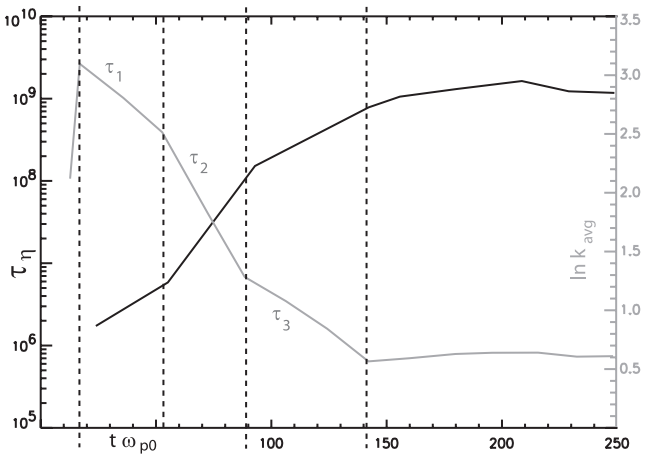

FIG. 4.—"Thermalization" timescale $\tau_\eta\omega_{p0}(t)$ for ohmic dissipation of the initial kinetic energy by "anomalous" particle transport and the time evolution of the average wavenumber $k_{\rm avg}(t)c/\omega_{p0}$ (*gray line*) in the magnetic field Fourier spectrum. Short field correlation scales (large $k_{\rm avg}$) directly correspond to strong cross-field diffusion (short τ_η). Typical correlation scale *e*-folding times for the regime of linear growth and/or current self-pinching $\tau_1\omega_{p0} \sim 60$ and self-pinch coalescence $\tau_3\omega_{p0} \sim 75$ result from the typical particle gyro times (meandering) $t_c\omega_{p0} = (2\epsilon_B)^{-1/2}$ in the self-generated field. In the intermediate phase $\tau_2\omega_{p0} \sim 25$ the time evolution is progressive because incipient current self-pinches are weakly shielded by their own toroidal field, and oppositely aligned filaments can cross each other. Here τ_η saturates at a point in time prior to the start of the analysis of the individual particle data in Fig. 3.

separated by $L \sim 10^2(c/\omega_{p0})$ in the final state, typical diffusion-limited lifetimes of

$$\tau_{\rm DL} = L^2/D_{\rm PIC} \sim 10^4(c/\omega_{p0})^2/9.6\times10^{-6}(c^2/\omega_{p0}) \sim 10^9\omega_{p0}^{-1}$$

result.

For the lower collision energy γ_0^{10} the current filament/magnetic field topology is much more complex because the parallel TSI mode contributes significantly. Filaments then show time-dependent three-dimensional modifications, structures saturate at smaller k, and typical separation distances decrease (Jaroschek et al. 2004a). The corresponding diffusion-limited lifetimes decay down to $\tau_{\rm DL}^{10}\omega_{p0} \sim 10^7$, suggesting that under certain conditions (see § 4) magnetic field lifetimes become insufficient to guarantee synchrotron emission. This result is in accord with the analysis of certain time-resolved GRB prompt emission spectra (Ghirlanda et al. 2003). In this reference, the comparison of observational data with the spectral shapes as expected from nonthermal emission models is unsatisfactory, indicating that internal magnetic fields live on a timescale that is short compared to synchrotron losses.

3.2. *Diffusion is Identified as "Bohm"-Type*

Collisionless cross-field diffusion was identified as Bohm-type in test-particle simulations of high-temperature (T) plasma in the limit of strong magnetic fields (B). Motivated as pervasive in fusion devices, such conditions imply Debye lengths to be larger than typical particle gyro radii $\lambda_D > \rho$. In this limit Dawson et al. (1971) associated Bohm-type behavior with anomalous particle collisions with electrostatic "convective cells." Chu et al. (1978) further identified contributions of a magnetostatic mode to retain $\propto T$-diffusion, and Lin et al. (1978) proved electrostatic fluctuations to be the dominant source of scattering. Diffusion is understood as Bohm-type if it exhibits the characteristic $D_B \propto T/B$-behavior. Bohm diffusion provides the most efficient cross-field transport possible, far more efficient than expected from a simple extrapolation of the "classical," collision-imposed $1/B^2$ dependence.

The Weibel instability is of interest in GRB scenarios in which the plasma outflow is kinetically dominated, i.e., $\lambda_D < \rho$ is valid. A fundamental question is, then, whether Weibel generated magnetic fields do also exhibit Bohm-type diffusion. Figure 5*a* shows the diffusion rate $(\Delta x)^2/\Delta t(1/B)$ plotted as a function of the inverse magnetic field at the respective particle position. The straight horizontal line is significant and clearly indicates Bohm-type $D_B \propto 1/B$ dependence, again directly obtained from the particle data. The ordinate value

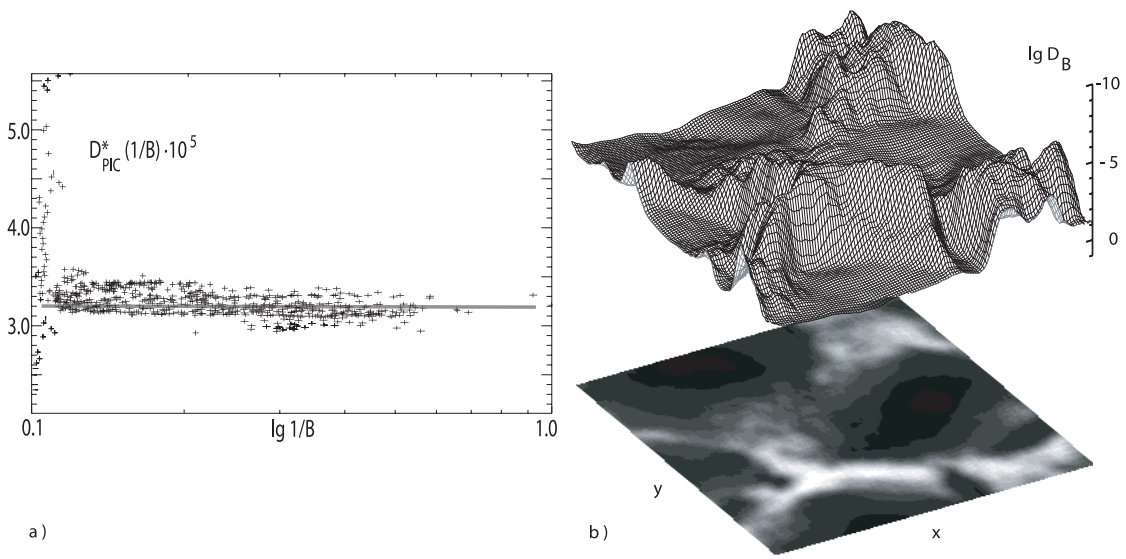

FIG. 5.—Microphysical diffusion coefficient $D^*_{\rm PIC}(1/B)$ as a function of $1/B$ for the individual particle already analyzed in Fig. 3*a*. The straight line indicates Bohm-type $1/B$ behavior derived from the line fit in Fig. 3*a* (which corresponds to the time average). The high fluctuations at small $1/B$ reflect the relation $\delta B/B \sim 1$ for the fluctuation scale height. Scattering around the straight line represents contributions from the meandering motion. The surface contours in (*b*) show the z-averaged Bohm diffusion coefficient $D_B = \alpha cT_\perp/eB$ derived from the perpendicular temperature $T_\perp$ (as the statistical quantity of the total ensemble of 5×10^8 simulated particles, $\alpha = 1$ assumed); $D_B \sim 10^{-5}(c^2/\omega_{p0})$ indicates $\alpha \sim 1 - 1/10$ in fine agreement with the "Maxwellian" $\alpha = 1/16$.

$(\Delta x)^2/\Delta t = 3.2\times10^{-5}\left(c^2/\omega_{p0}\right)$ coincides with the slope of the line fit obtained for the same particle in Figure 3*a*. With this insight obtained, we look for the ratio of $D_B = \alpha cT_\perp/eB$ as characteristic of the Bohm diffusion and α representing only an insignificant dimensionless correction factor. Setting $\alpha = 1$ and calculating the perpendicular temperature $T_\perp = \int d\boldsymbol{p} p_\perp v_\perp f(\boldsymbol{p})$ as defined in the relativistic energy–momentum tensor, D_B surface contours are shown in Figure 5*b*. As a third and absolutely consistent constraint on the cross-field diffusion, $D_B \sim 10^{-6}(c^2/\omega_{p0})$ is reached as the maximum (time-limiting) value located in the walls of magnetic confinement (cf. Fig. 2).

As a provocative conjecture, one could infer a general mechanism of "minimum action" governing the complete scenario: Ab initio, the system contains its free energy in the directed motion of plasma shells. The final objective is the maximum enthalpy gain via thermalization. Two plasma instability channels are possible: (1) the TSI mode with parallel electric fields broadens the initially sharply defined bulk motion, and (2) the WBI mode introduces magnetic fields responsible for isotropization. The coupling of the two modes is energy-dependent. For progressively higher energies WBI contributions dominate, resulting in the magnetically confined (quasi-) steady state configuration that is final on timescales feasible in PIC simulations. Nevertheless, Bohm-type transport is accomplished as the most efficient "anomalous" thermalization process.

4. CONSEQUENCES FOR SYNCHROTRON EMISSION

As the net effect of all microphysical diffusion processes the lifetime of Weibel magnetic fields is limited to $\tau_{\rm DL}\omega_{p0} \sim 10^9$. Albeit the presented simulations refer to (e^+, e^-) shell collisions, the results directly transfer to the case of "baryonic" contributions; Nishikawa et al. (2003) and Frederiksen et al. (2004) investigated the Weibel instability for relativistic collisions of electron–proton (*e*, *p*) shells. Although applying an artificial mass ratio of just $m_p/m_e = 16$, magnetic field generation and plasma heating via the WBI-TSI mode are spatially and temporally decoupled by a relative factor of $f_r = (m_p/m_e)^{1/2}$, and lower hybrid contributions appear to be negligible. Simulation of the real mass ratio in three-dimensional scenarios is beyond the scope of contemporary supercomputers, but the decoupling is expected to be even more pronounced for higher mass ratios. Comparable bulk energies γ_0 yield equivalent equipartition ratios $\epsilon_{B,e} \sim \epsilon_{B,p}$ for each of the species. Consequently, protons give dominant ($\propto f_r$) contributions to the Weibel current filament/magnetic field structure. Electrons are strongly thermalized, modify the field structure in the subpercent regime, and merely serve as the charge- and current-neutralizing element. However, electrons further represent the dominant source of synchrotron emission in the proton-sustained Weibel fields.

With the Weibel mechanism as the connection between plasma kinetic quantities (n_0, γ_0) and the generated magnetic field (ϵ_B, B_0), typical synchrotron cooling times can be formulated in units of plasma inertial timescales,

$$\tau_{\rm sc}\omega_{p0} = 3.5\times10^{17}\gamma_0^{-1}(\gamma_0-1)^{-1}(n/1\ {\rm cm}^3)^{-1/2}\epsilon_B^{-1/2}(m/m_e)^{-3/2}.$$

According to Figure 1, $\epsilon_B^{10} \sim 2.5\%$ and $\epsilon_B^{100} \sim 10\%$ result as final steady state conditions in the highly nonlinear regime. Apparently the mass ratio m/m_e is important. Being unity for (e^+, e^-) shells, it represents the fact that, in the case of baryonic contributions, magnetic field generation and diffusive decay take place on ion scales, while radiative cooling is appendant to lepton scales. Distinguishing between GRB prompt emission as the result of internal collisions associated with plasma densities $n_0^{\rm int} \sim 10^{10}$–$10^{16}$ cm^{-3} and afterglow in external collisions with the ambient medium in the regime $n_0^{\rm ext} \sim 10^0$–10^2 cm^{-3}, typical observed timescales, $\tau_{\rm int} = 10^{-3}$–10^{-1} s and $\tau_{\rm ext} = 10^1$–10^4 s, correspond to typical plasma inertial scales, $\tau_{\rm int}\omega_{p0} \approx \tau_{\rm ext}\omega_{p0} \sim 10^5$–$10^{10}$. In the general scheme, internal collisions are associated with (e^+, e^-) fireball ejecta (Piran 1999) and external collisions in the "standard" afterglow model (Panaitescu & Kumar 2002) with the (*e*, *p*) plasma of the ambient medium. Beloborodov (2002) argues convincingly that (1) internal (e^+, e^-) plasma should contain a baryonic pollution because otherwise the observational fact of comparable energy deposition for prompt emission and afterglow is unbalanced toward early times, and (2) external (*e*, *p*) plasma should possess a leptonic pollution because of the impact of the prompt γ-ray blast on the ambient medium, a facet not covered in the standard afterglow model.

Employing the PIC simulation's self-consistent equipartition ratios, typical synchrotron cooling times are calculated to $\tau_{\rm sc,10}^{\rm int}\omega_{p0} = 10^8$–$10^{11}$, $\tau_{\rm sc,100}^{\rm int}\omega_{p0} = 10^6$–$10^9$ ($\tau_{\rm sc,10}^{\rm int}\omega_{p0} = 10^3$–$10^6$, $\tau_{\rm sc,100}^{\rm int}\omega_{p0} = 10^1$–$10^4$), and $\tau_{\rm sc,10}^{\rm ext}\omega_{p0} = 10^{15}$–$10^{16}$, $\tau_{\rm sc,100}^{\rm ext}\omega_{p0} = 10^{13}$–$10^{14}$ ($\tau_{\rm sc,10}^{\rm ext}\omega_{p0} = 10^{10}$–$10^{11}$, $\tau_{\rm sc,100}^{\rm ext}\omega_{p0} = 10^8$–$10^9$) for $\gamma_0 = 10$ and 100, respectively. As soon as baryonic contributions are significant, the mass ratio becomes important ($\tau_{\rm sc}$ values in parentheses). The corresponding synchrotron cutoffs in the collision frame $\omega_{\rm cut}/\omega_{p0} = 3\sqrt{2}(\gamma_0-1)^{1/2}\gamma_0^2\epsilon_B^{1/2}$ range around $\omega_{\rm cut,100}^{\rm int} \sim 10^{14}$–$10^{18}$ Hz and $\omega_{\rm cut,100}^{\rm ext} \sim 10^{10}$–$10^{11}$ Hz. Cutoff frequencies are less sensitive to density variations and/or baryonic contributions and suggest an energy range $\gamma_0 \sim 10^2$ for both internal and external collisions, thereby giving credit to conjectures that variabilities in the shells' bulk momentum range around the respective absolute momentum $\Delta\gamma/\gamma_0 \sim 1$.

In conclusion, typical synchrotron cooling times $\tau_{\rm sc}\omega_{p0} \lesssim 10^9 \sim \tau_{\rm DL}$ are shorter than the diffusion-limited lifetimes of Weibel fields for sufficiently high collision energies $\gamma_0 \sim 10^2$. The energetic constraint relaxes for higher densities and baryonic contributions; the latter appear most likely. Furthermore, the generation of Weibel fields up to the steady state configuration takes place within $\tau\omega_{p0} \lesssim 10^2$, i.e., is instantly fast with respect to diffusive decay and synchrotron emission. Plasma shells in a real GRB scenario are expected to be far more extended in the direction of bulk motion, which relates to a simulation setup that is continuously pumped by an injected plasma beam (see Frederiksen et al. 2004, especially their Fig. 5). In an open, beam-powered system, diffusive losses are readily compensated, extending the diffusion limit by the respective beam lifetime.

In conclusion, PIC simulations serve to identify the stability of Weibel scenarios by self-consistent analysis of magnetic cross-field diffusion. The diffusion process is identified as Bohm-type, which is the fastest diffusive decay mechanism possible. Hence, the typical diffusion-limited lifetime of the Weibel fields in plasma shell collisions represents a merely conservative limit around $\tau_{\rm DL}\omega_{p0} \sim 10^9$. Such a stability appears sufficient to validate synchrotron emission scenarios for GRB prompt emission as well as afterglow, especially in view of likely baryonic contributions to the pair-plasma and plasma shells, which are much more extended in the parallel direction than imposed by the computational limits of the PIC simulations.

The authors thank S. Matsukiyo, K. Hallatschek, and M. Scholer for fruitful discussions, the Max Planck Rechenzentrum Garching and Leibniz Rechenzentrum Munich for the granted computation time. The work of C. H. J. was performed under the auspices of the International Max Planck Research School on Astrophysics. R. T. thanks the International Space Science Institute Bern for hospitality during a Senior Visiting Scientist term.

REFERENCES

Beloborodov, A. M. 2002, Proc. of the Conf. on Compact Stars in the QCD Phase Diagram, ed. R. Ouyed & F. Sannino (Copenhagen: Nordic Inst. Theor. Phys.), http://www.slac.stanford.edu/econf/C010815/index.html
Birdsall, C. K., & Langdon, A. B. 1995, Plasma Physics via Computer Simulation (2nd. ed.; New York: McGraw-Hill)
Chu, C., Chu, M., & Ohkawa, T. 1978, Phys. Rev. Lett., 41, 653
Dawson, J. M., Okuda, H., & Carlile, R. N. 1971, Phys. Rev. Lett., 27, 491
Frederiksen, J. T., Hededal, C. B., Haugbolle, T., & Nordlund, A. 2004, ApJ, 608, L13
Ghirlanda, G., Celotti, A., & Ghisellini, G. 2003, A&A, 406, 879
Gruzinov, A. 2001, ApJ, 563, L15
Jaroschek, C. H., Lesch, H., & Treumann, R. A. 2004a, ApJ, 616, 1065
———. 2004b, ApJ, 605, L9
Jokipii, J. R., Kóta, J., & Giacalone, J. 1993, Geophys. Res. Lett., 20, 1759
Kazimura, Y., Sakai, J. I., Neubert, T., & Bulanov, S. V. 1998, ApJ, 498, L183
Lee, R., & Lampe, M. 1973, Phys. Rev. Lett., 31, 1390
Lin, A. T., Dawson, J. M., & Okuda, H. 1978, Phys. Rev. Lett., 41, 753
Medvedev, M. V, & Loeb, A. 1999, ApJ, 526, 697
Mészáros, P. 2002, ARA&A, 40, 137
Nishikawa, K.-I., Hardee, P., Richardson, G., Preece, R., Sol, H., & Fishman, G. J. 2003, ApJ, 595, 555
Panaitescu, A., & Kumar, P. 2002, ApJ, 571, 779
Piran, T. 1999, Phys. Rep., 314, 575
Sagdeev, R. Z. 1979, Rev. Mod. Phys., 51, 1
Silva, L. O., Fonseca, R. A., Tonge, J. W., Dawson, J. M., Mori, W. B., & Medvedev, M. V. 2003, ApJ, 596, L121
Taylor, J. B., & McNamara, B. 1971, Phys. Fluids, 14, 1492
Weibel, E. S. 1959, Phys. Rev. Lett., 2, 83